Article

A Predictive Computational Model of the Dynamic 3D Interphase Yeast Nucleus

Hua Wong,[1,4,6] Hervé Marie-Nelly,[1,4,5,6]
Sébastien Herbert,[1,4,6,8] Pascal Carrivain,[3,4] Hervé Blanc,[2,4,7]
Romain Koszul,[2,4,7] Emmanuelle Fabre,[2,4,7]
and Christophe Zimmer[1,4,6,*]

[1]Institut Pasteur, Groupe Imagerie et Modélisation,
75015 Paris, France
[2]Institut Pasteur, Laboratoire Régulation Spatiale du Génome,
75015 Paris, France
[3]CNRS, LPTMC, UMR 7600
[4]CNRS, GDR 3536
Université Pierre et Marie Curie, 75252 Paris, France
[5]Université Pierre et Marie Curie, Cellule Pasteur,
75015 Paris, France
[6]CNRS, URA 2582, 75015 Paris, France
[7]CNRS, UMR 3525, 75015 Paris, France
[8]Université Paris Diderot, Sorbonne Paris Cité, Cellule Pasteur,
75015 Paris, France

Summary

Background: Despite the absence of internal membranes, the nucleus of eukaryotic cells is spatially organized, with chromosomes and individual loci occupying dynamic, but nonrandom, spatial positions relative to nuclear landmarks and to each other. These positional preferences correlate with gene expression and DNA repair, recombination, and replication. Yet the principles that govern nuclear organization remain poorly understood and detailed predictive models are lacking.
Results: We present a computational model of dynamic chromosome configurations in the interphase yeast nucleus that is based on first principles and is able to statistically predict the positioning of any locus in nuclear space. Despite its simplicity, the model agrees with extensive previous and new measurements on locus positioning and with genome-wide DNA contact frequencies. Notably, our model recapitulates the position and morphology of the nucleolus, the observed variations in locus positions, and variations in contact frequencies within and across chromosomes, as well as subchromosomal contact features. The model is also able to correctly predict nuclear reorganization accompanying a reduction in ribosomal DNA transcription, and sites of chromosomal rearrangements tend to occur where the model predicted high contact frequencies.
Conclusions: Our results suggest that large-scale yeast nuclear architecture can be largely understood as a consequence of generic properties of crowded polymers rather than of specific DNA-binding factors and that configurations of chromosomes and DNA contacts are dictated mainly by genomic location and chromosome lengths. Our model provides a quantitative framework to understand and predict large-scale spatial genome organization and its interplay with functional processes.

*Correspondence: czimmer@pasteur.fr

Introduction

Besides the one-dimensional information carried by the nucleotide sequence, the three-dimensional arrangement of the genome in the nucleus of eukaryotic cells emerges as an important determinant of gene expression, DNA repair, recombination, and replication [1]. Although they lack any membrane apart from the nuclear envelope, nuclei from yeast to humans exhibit strong compartmentalization into nuclear bodies and other functionally distinct subdomains. In metazoans, chromosomes are confined to nonoverlapping territories, whose relative positions in the nucleus are not random [2]. Individual loci occupy preferential, though dynamic, positions with respect to their chromosome territory or other nuclear landmarks such as the nuclear envelope or the nucleolus [3, 4]. These positioning patterns affect the transcriptional status of genes, and the nucleus appears compartmentalized in domains that either favor or silence gene expression [5]. Cancer-promoting chromosomal rearrangements arise from illegitimate fusions between broken parts of the same or distinct chromosomes. In mammals, some of these events occur preferably at pairs of genomic locations that are more frequently in contact and are thus affected by spatial positioning of chromosomal regions [6–10]. Conversely, in yeast, many loci move to new subnuclear positions or change their dynamics upon changes in their expression or as a result of DNA breaks [5, 11–14].

Despite such functional relevance, the main factors and mechanisms that control dynamic nuclear organization are presently ill understood. These can be divided into two broad classes [15]. A first class includes protein complexes, such as CTCF, which bind to particular discrete DNA sequence motifs and promote their interaction with nuclear landmarks or distal loci, thus restricting subnuclear positions or forming loops or interchromosomal attachments [16, 17]. In a second class are generic effects arising from the properties of semiflexible polymers (chromosomes) confined to the crowded nuclear volume. Generic properties have been proposed to explain, for example, the formation of chromosome territories, and the aggregation of large macromolecular complexes in the nucleus [18, 19]. Although both specific factors and generic effects are present, their relative contributions remain unclear and a detailed predictive model of nuclear organization is not yet available.

The well-studied budding yeast *Saccharomyces cerevisiae* provides an attractive model to study nuclear organization and its functional relevance. Electron microscopy has revealed structural nuclear landmarks [20]; light microscopy has allowed to map the positions and dynamics of selected loci in individual nuclei [3, 21–25]; and a chromosome conformation capture (3C) assay [26] coupled with massive DNA sequencing (Hi-C) has provided a matrix of contact frequencies across the genome [27]. Despite its small diameter (~ 2 μm), the yeast nucleus is characterized by strong functional compartmentalization [3, 5, 15]. The most prominent nuclear compartment is the nucleolus, the site of transcription of ribosomal RNA genes (rDNA), consisting of ~ 100–200 tandem repeats on the right arm of chromosome 12. In *S. cerevisiae*, the nucleolus is

a single, crescent-shaped structure abutting the nuclear envelope, encompassing roughly 1/3 of the nuclear volume, and excluding the bulk of the genome except for the rDNA [20, 22, 27]. What determines the position and shape of the nucleolus, as well as its segregation from the rest of the genome, remains unknown.

The budding yeast nucleus is further characterized by a distinct Rabl-like chromosome configuration, in which each chromosome's centromere is tethered by a single microtubule and the kinetochore complex to the spindle pole body (SPB), a multiprotein complex embedded in the nuclear envelope and located opposite of the nucleolus [3, 28]. Telomeres are tethered to the nuclear envelope via redundant pathways [29]. Their spatial position in the nucleus, as well as that of internal loci, correlates with genomic distance from the centromere [3, 22]. These data are qualitatively consistent with a relatively simple configuration of chromosomes governed by generic physical constraints [15]. By contrast, much more complex configurations, with the chromatin fiber crisscrossing the nucleus, have been proposed based on the reported colocalization of genes such as transfer RNA [30]. How exactly the chromatin fiber is organized in 3D yeast nuclear space thus remains unclear.

Contact frequencies measured by Hi-C have been used to construct a static, and more recently, a dynamic 3D model of yeast chromosomes in the nucleus [27, 31]. The dynamic model was found to be consistent with measurements of distances between telomeres [21]. However, both models [27, 31] assumed untested relationships between spatial distances and contact frequencies, and the dynamic model assumed an artificial nucleolar compartment [31]. As they rely on experimental data, such models cannot predict how nuclear organization changes in different experimental conditions.

Here, we present a predictive quantitative model of dynamic chromosome arrangements in the yeast nucleus. Our model is based on first principles rather than derived from imaging or Hi-C data. Nonetheless the model recapitulates observed patterns of intranuclear locus positioning and chromatin contacts across the genome. In addition, our model correctly predicted an alteration of nuclear architecture in response to a reduction of rDNA gene expression, and may be used in the future to predict the propensity of different pairs of loci to undergo recombination.

Results

Computational Model of Dynamic Yeast Chromosomes

We built a computational simulation of chromosome configurations and their dynamics in the yeast nucleus (Figure 1; see Figure S1 and Movie S1 available online). Details are provided in the Experimental Procedures. We considered a nominal model and three control models (Tables 1 and 2). Briefly, we modeled the 16 chromosomes of haploid yeast as freely jointed chains of segments characterized by constant diameter, compaction, and rigidity parameters (Figure 1A; Table 1). Our nominal model reflects the specific nature of the rDNA chromatin (heteropolymer model). At the rDNA locus, ribosomal subunits are assembled cotranscriptionally, leading to strong accumulation of RNA and proteins [20]. To account for this, we increased the diameter of the rDNA segments, such that the effective volume occupied by rDNA was ∼1/3 of the nucleus (Figure 1B; Table 1). Each chromosome was linked to the SPB at its centromere by a single rigid microtubule (Figure 1C–1E). The telomeric ends were maintained

near the nuclear envelope (represented by a spherical shell) by an outward force, but allowed to move freely along its surface. Assumed parameter values were based on the literature and are summarized in Table 1. Chromosomes were subjected to random thermal motions only (Movie S1). The model incorporated topological constraints, such that chain segments could not penetrate each other. From the simulated families of dynamic chromosome configurations (Figure S1I), we then computed several features of nuclear organization, including intranuclear distributions for any locus (Figure S1J), distances between any pair of loci (Figure S1K), and contact frequencies between any pair of chromosomal regions (Figure S1L). For comparisons, we also considered three control models: (1) a phantom model in which topological constraints were removed, (2) a homopolymer model in which all chromosomes, including the rDNA, had the same properties (except their genomic length), and (3) a microtubule-free model, in which centromeres were not linked to the SPB (Table 2).

Model Recapitulates Formation of the Nucleolar Compartment and Quantitative Locus Positions

As a first test of our model, we compared the predicted subnuclear locations of selected loci to those obtained from imaging experiments [3, 22] (Figure 2). These positions can be visualized as probability maps in a coordinate system ($R \cos \alpha$, $R \sin \alpha$), where R is the radial distance to the center of the nucleus, and α is the angle with respect to the axis joining the nuclear and nucleolar centers [3] (Figure S1J). In our nominal model, centromeres occupied territories roughly halfway between the SPB and the nuclear center, whereas telomeres distributed themselves at the nuclear periphery, in accordance with observations (Figures 2A–2E, 2G–2K). This is unsurprising because our model tethered centromeres to the SPB via microtubules and tethered telomeres to the nuclear envelope. By contrast, the subnuclear location of other loci was not built in. Remarkably, our model predicted that the rDNA locus displayed a crescent-shape distribution abutting the nuclear envelope and a position opposite the SPB (Figure 2F). This morphology was strikingly similar to the rDNA territory determined by light microscopy (Figure 2L) and to the dense nucleolus observed by electron microscopy [3, 20]. The model predicted that all DNA except the rDNA is excluded from the nucleolus, such that the telomeres of even long arms cannot extend to the face opposite the SPB, in agreement with experimental data [3, 22]. By contrast, the control models failed to reproduce the territories of at least some loci: both the phantom model and the homopolymer model led to strikingly different patterns of localization (Figures 2A'–2F' and 2A"–2F"), whereas the microtubule-free model failed to position the rDNA opposite the SPB (Figures 2A"' and F"'). Thus, our heteropolymer model qualitatively recapitulates experimentally observed features of nuclear organization, notably the morphology of the nucleolus, and the segregation of the rDNA from the rest of the genome.

We next turned to a more quantitative test of predicted locus positions. First, we analyzed the "absolute" intranuclear positions of selected loci. Because data from previous studies [3, 22] included mostly loci on different chromosomes, we performed new imaging experiments on 16 loci distributed along the right arm of chromosome 4, the second longest arm after the rDNA-carrying right arm of chromosome 12 (Table S1). Our data set encompassed 36 loci on 13 out of the 16 chromosomes and included two loci on the right arm of chromosome 12. We first compared the predicted median angles α to
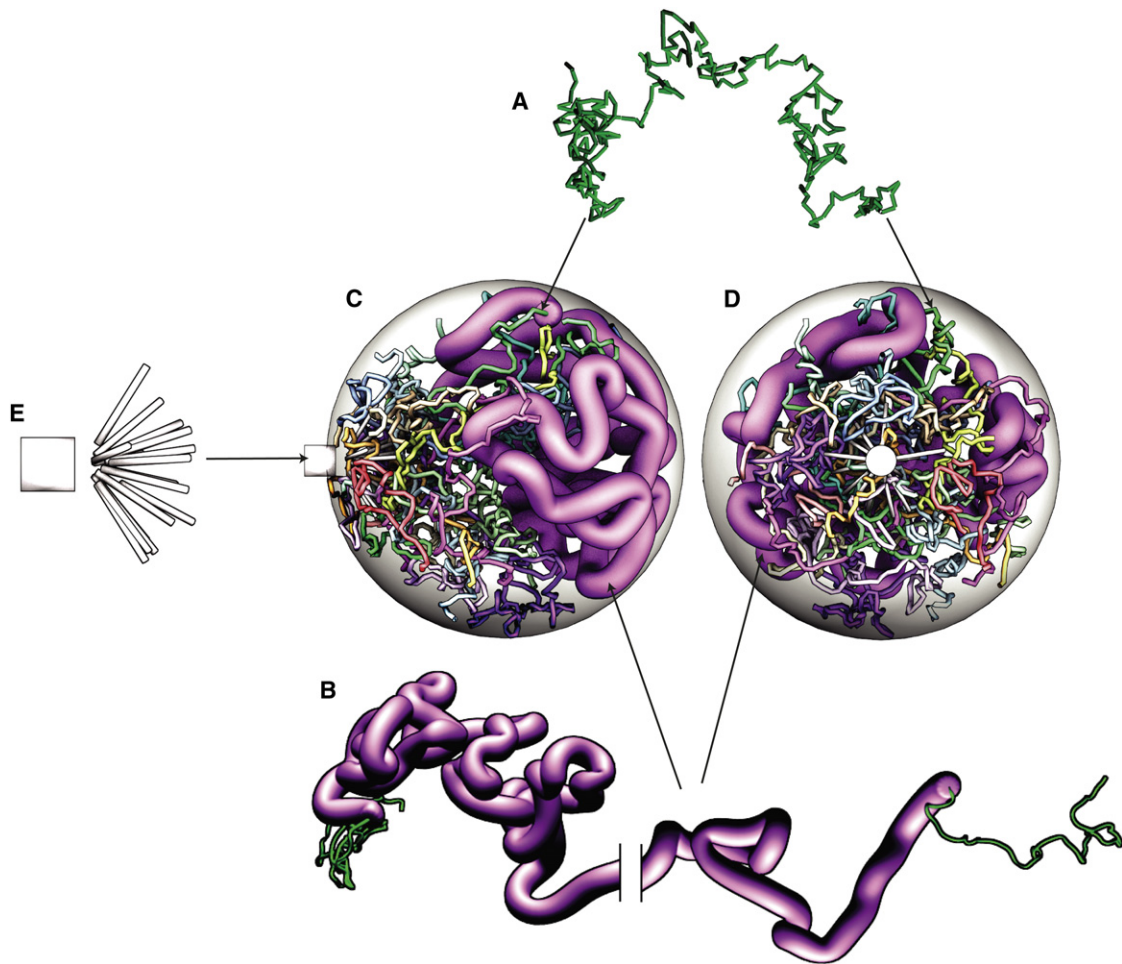
Figure 1. Computational Model of the Dynamic Interphase Yeast Nucleus

(A) Each chromosome is represented as a self-avoiding articulated chain of rigid segments.

(B) The heterochromatic rDNA locus on chromosome 12 is represented by thicker segments (pink, displayed using surface smoothing) than the rest of the DNA (green).

(C and D) A snapshot of the full model, showing each of the 16 chromosomes in a different color. The sphere represents the nuclear envelope. Two orthogonal views are shown: (C) view perpendicular to the axis joining the nuclear center to the SPB and (D) view along this axis and facing the SPB.

(E) The SPB (white knob) and the 16 microtubules, represented each by one rigid segment. See also Figure S1 and the animated simulation in Movie S1.

measurements. Overall, predicted angles correlated remarkably well with the measurements (Pearson's r = 0.87; p < 10^{-11}), despite an underestimation of ≈ 18 deg (Figure 2M). The model predicted that α correlated with genomic distance to the centromere (d_{CEN}) (Figure S2A). This correlation had previously been observed for telomeres [22], but our new measurements showed that it also extends to internal loci, as predicted by the model (Figure S2B). The model further predicted that loci on the rDNA carrying arm of chromosome 12 (*GAL2* and rDNA) have larger α than other loci of similar d_{CEN} (Figure S2A). This was again borne out by measurements (Figure S2B).

We next considered the positioning of loci relative to each other. Because only the centromeres are tethered to a specific point, we reasoned that the most sensitive test of the model was for loci most distal from centromeres, i.e., the telomeres. We therefore compared our model's predictions against the 3D distances previously measured between 63 distinct pairs of subtelomeres [22], each of which contained one of three subtelomeres (6R, 10R, 4R), belonging to a short (122 Kb),

middle (310 Kb), and long (1,050 Kb) chromosome arm, respectively. The correlation between predicted and measured distances was good (r = 0.65, p < 10^{-7}), despite an underestimation by the model of ~150 nm (Figure 2N). The predicted distances strongly depended on the lengths of the two chromosome arms, in a manner approximately similar to that observed in experiments [22] (Figure S2C–S2H). For short or medium arms, the two extremities of the same chromosome were predicted to be closer than for pairs of arms with similar lengths on different chromosomes (Figures S2C and S2E), also in agreement with measurements (Figures S2D and S2F) [22].

In comparison to the nominal model, the homopolymer and phantom models both failed to explain the measured angles α (Figures S2J and S2K) but predicted distances between telomeres also agreed with measurements (Figures S2N and S2O). The microtubule-free model failed to explain both angles and distances (Figures S2L and S2P) (Table 2). Thus, only the nominal model quantitatively accounts for absolute locus positions and the relative positions of telomeres.

Table 1. Parameters of the Nominal Simulation

Parameter	Value
Number of chromosomes and microtubules	16
Chromosome segment length (Kuhn length), L	60 nm
Nuclear radius, R_0	1 μm
Length of microtubules (+kinetochore), L_{MT}	380 nm
DNA compaction in chromatin, C	83 bp/nm
Diameter of euchromatin segments, D_0	20 nm
Diameter of rDNA segments, D_{rDNA}	200 nm
Number of rDNA segments, N_{rDNA}	150
Segments can cross each other	No

Model Recapitulates Contact Patterns of Chromosomes and Chromosome Arms

Whereas imaging provides detailed information on positions of a limited number of loci, Hi-C data allowed us to test the model on a genome-wide scale [27]. We first analyzed contact frequencies at the genomic scales of entire chromosomes (230–1,500 Kb) (Figure 3) and chromosome arms (80–1,050 Kb) (Figure S3). We considered the probability for a contact to occur between any pair of chromosomes (including within the same chromosome). In absence of any nuclear organization (i.e., if all pairs of loci in the genome randomly contact each other with uniform probability), this probability is the product of the chromosome's genomic lengths (Figure 3A). In this case, only 14.0% of all contacts should be intrachromosomal (cis) (Figure 3E). In reality, 53.0% of experimentally detected contacts are cis (Figures 3C and 3E), indicating strong departure from a random collision scenario. Our nominal model, however, predicted 53.7% of cis contacts, in remarkable agreement with experiments (Figures 3B and 3E). The correlation between predicted and measured probabilities was very high (Pearson's r = 0.99, Spearman ρ = 0.96, p < 10^{-50}), indicating that the overall distribution of contacts among chromosomes was well recapitulated by our model (Figure 3D). The model was also in good agreement with contact probabilities measured between pairs of chromosome arms (Figures S3A–S3D). Here, three types of contacts exist: (1) between arms on different chromosomes, (2) within each arm, (3) between left and right arms of the same chromosomes. Unlike the random collision model, the nominal chromosome model predicted proportions of these three contact types in relatively good agreement with experimental data (Figure S3E).

However, we noted that, if taken separately, probabilities for interchromosomal contacts (trans) also agreed very well with the random collision scenario (r = 0.82, ρ = 0.88, p < 10^{-30}) (Figures 3A and 3C); a similar result held for chromosome arms (r = 0.87, ρ = 0.88, p < 10^{-50}) (Figures S3A and S3C). This suggested that, to first approximation, contacts

between different chromosomes or arms occur indiscriminately. To remove this effect, we next computed contact probabilities averaged over the product of the genomic lengths for each pair of chromosomes (or arms) (Figures 3F–3I; Figures S3F–S3I). Because random collisions predicted uniform average contact frequencies (Figure 3F; Figure S3F), any deviations from constancy reflect nonrandom nuclear organization. Overall, the average contact frequencies between chromosomes (cis + trans) predicted by the model still correlated very well with measurements (r = 0.97, ρ = 0.80, p < 10^{-50}) (Figures 3G–3I). This was also true for contacts between arms (r = 0.91, ρ = 0.86, p < 10^{-50}) (Figures S3G–S3I). Taken separately, the 16 predicted cis contact frequencies were also in very good agreement with measurements (r = 0.91, ρ = 0.94, p < 10^{-5}) (Figure 3I). There was likewise good agreement for contacts within each of the 32 chromosome arms (r = 0.69, ρ = 0.73, p < 10^{-4}) (Figure S3I). Most significantly, the predicted trans contact frequencies of chromosomes, taken separately, also correlated very well with the measurements (r = 0.84, ρ = 0.72, p < 10^{-30}) (Figure 3I), as did predicted contacts between arms of different chromosomes (r = 0.86, ρ = 0.82, p < 10^{-50}) (Figure S3I). The trans frequencies agreed well, although less so, with those predicted by the homopolymer model (r = 0.63, ρ = 0.52 for chromosomes, r = 0.79, ρ = 0.73 for arms), but not with those predicted by the microtubule-free model (r = −0.004, p = 0.97; ρ = −0.03, p = 0.72 for chromosomes, r = 0.04, p = 0.42; ρ = 0.12, p = 0.01 for arms) (Figures S2R, S2S, S2U, and S2V) (Table 2). Note that the phantom model by definition did not predict any contacts.

Thus, our nominal model largely recapitulates genome-wide contact frequencies at the scale of entire chromosomes or chromosome arms.

Contact Frequencies at Subchromosomal Scales

Next, we considered contact frequencies at the maximum resolution afforded by our model, i.e., in 5 Kb bins. At this genomic resolution, the experimental contact matrix is very sparse, with on average only 1.4 contacts per bin, leading to strong counting noise (mean coefficient of variation [c.v.] 1.4$^{-1/2}$ = 0.84, compared to 131 contacts per bin and c.v. < 0.1 for the predicted matrix). The full predicted contact matrix correlated only weakly with its experimental counterpart (r = 0.24) (Figures S4A and S4B). However, trading off genomic resolution to reduce statistical noise strongly improved the correlation, which reached r = 0.85 for bins of 75 Kb (Figure S4C).

Both predicted and measured intrachromosomal matrices are dominated by a strong diagonal, i.e., by contacts between genomically proximal loci, as expected for polymers with

Table 2. Simulations Considered and Assessment of Their Predictions

Model	Difference with nominal simulation	Agreement with experimental data			
		Subnuclear probability maps	Absolute positions (α)	Relative telomere positions	Average interchromosomal contacts
Nominal	None	+	+	+	+
Phantom	Segments can cross	−	−	+	NA
Homopolymer	$D_{rDNA} = D_0$	−	−	+	+
Microtubule-free	No tethering to SPB	−	−	−	−

This table lists the nominal model and the three control models and indicates how their predictions agree with different measurements. Symbols + and − indicate good and poor agreement between model and measurements, respectively. See text and Figures 2, 3, S2, and S3 for quantifications. NA, not applicable (no contact frequencies are scored for the phantom model).
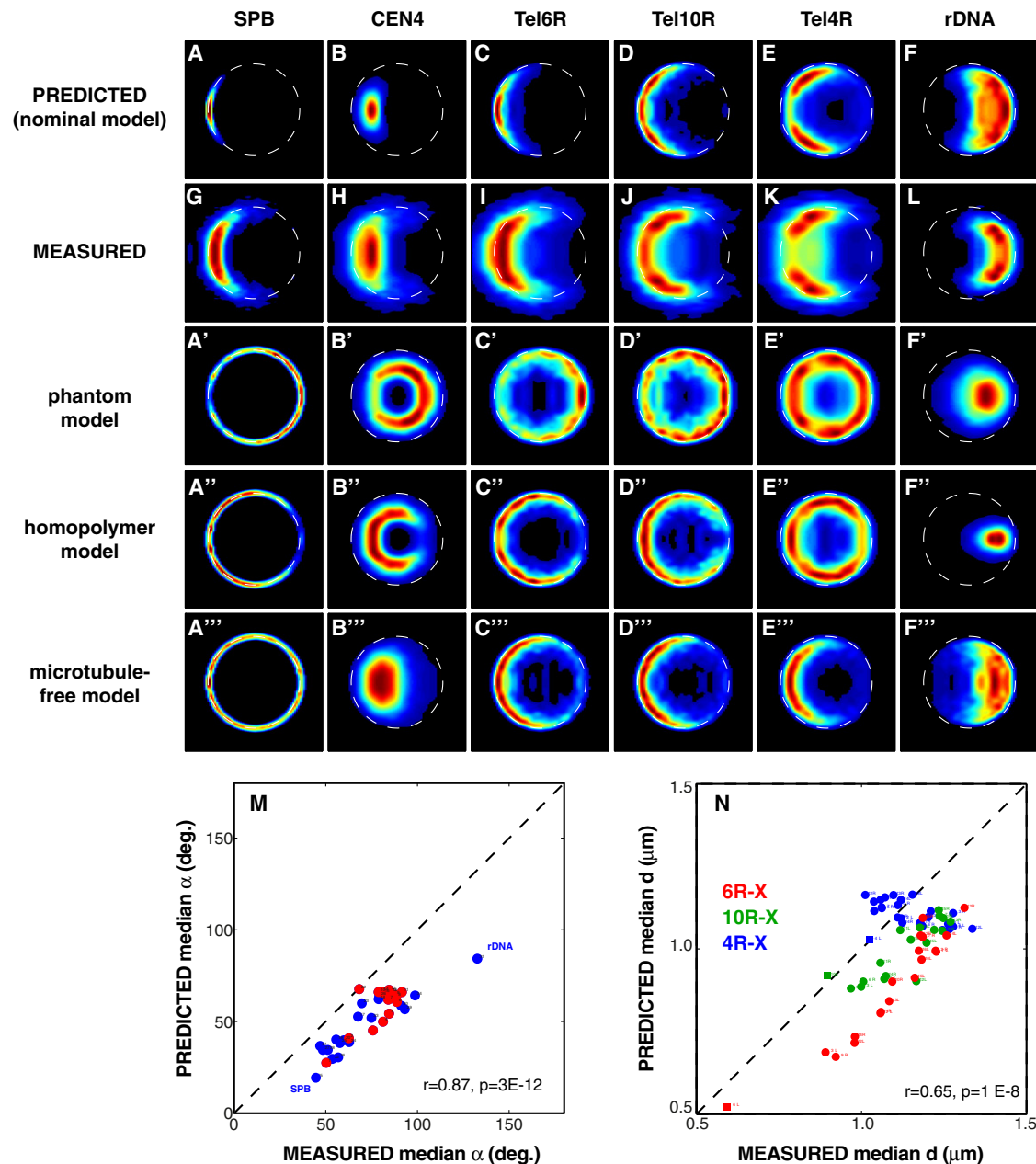
Figure 2. Model Recapitulates Nuclear Compartmentalization, Absolute, and Relative Locus Positions

(A–L, A'–F', A"–F", and A'''–F''') Nuclear territories of selected genomic loci and the SPB, visualized as probability maps. (A)–(F) show territories predicted by the nominal model; (G)–(L) show territories measured from light microscopy data [3, 22]; (A')–(F') show territories predicted by the phantom model; and (A")–(F") show territories predicted by the homopolymer model. Probability maps were obtained and displayed as described in [3] and Figure S1 J. Dashed circles have a fixed radius of 1 μm. Territories shown in each column, from left to right, correspond to: the SPB (A, G, A', A", A'''); the centromere of chromosome 4 (CEN4) (B, H, B', B", B'''); the telomere on the 122 Kb long right arm of chromosome 6 (Tel6R) (C, I, C', C", C'''); the telomere on the 310 Kb long right arm of chromosome 10 (Tel10R) (D, J, D', D", D'''); the telomere on the 1,050 Kb long right arm of chromosome 4 (Tel4R) (E, K, E', E", E'''), and an rDNA repeat (rDNA) (F, L, F', F", F'''). Note the good agreement between observed territories and those predicted by the nominal model, but not the control models. (M) and (N) show quantitative comparisons of predicted (nominal model) and measured absolute and relative locus positions. (M) shows predicted versus measured median angle α with respect to the nucleolar-nuclear axis. Each dot corresponds to a distinct locus as indicated by its number and Table S1. Red dots indicate loci along chromosome 4 that are new to this study; blue dots are data from previous work [3, 22].

(N) Predicted versus measured median distances between 63 pairs of telomeres. Each dot corresponds to a different pair of telomeres. Pairs containing the reference telomere 6R, 10R, or 4R have red, green and blue dots, respectively; the chromosome arm carrying the other telomere is indicated next to the dot (e.g., "3L" designates the left arm of chromosome 3). Squares indicate pairs of telomeres belonging to the same chromosome. See also Figure S2.

persistence lengths larger than the genomic resolution. We first analyzed how contact frequencies F between pairs of loci on the same chromosome fall off with genomic separation s (in Kb). Our model predicted that $F(s)$ decayed approximately as $s^{-1.5}$ between ~5 Kb and ~1,000 Kb, and was roughly constant beyond (Figure 4A). This is as expected for equilibrated confined polymers [32, 33] and differs from the s^{-1} decay observed in mammalian cells and attributed to an
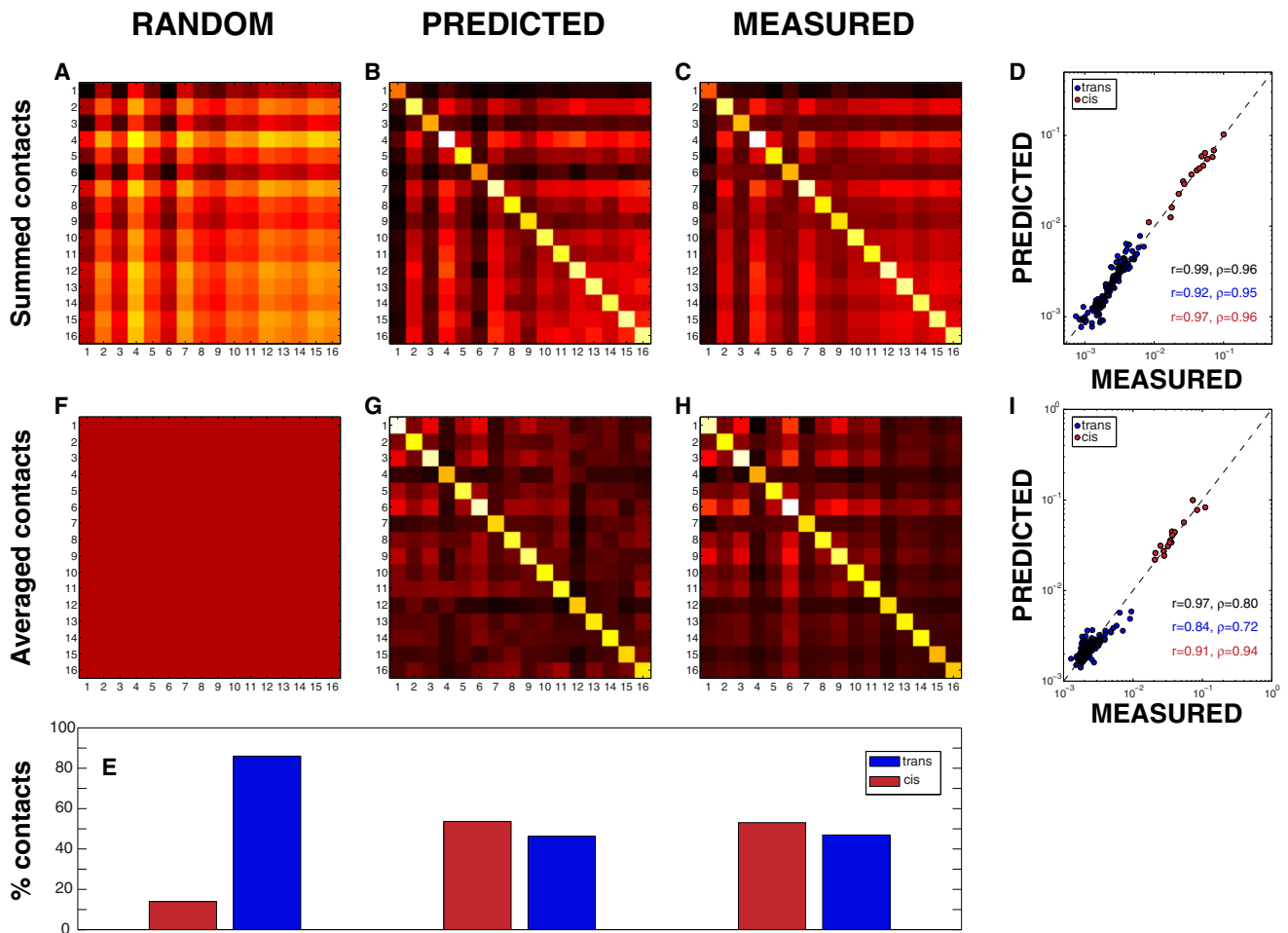
Figure 3. Model Recapitulates Patterns of Contacts among Chromosomes

(A–C, F–H) Contact frequency matrices for each pair of the 16 chromosomes. Chromosome numbers increase from top to bottom and from left to right. All matrices are displayed using the same logarithmic color scale, with dark colors indicating low probabilities, and bright colors high probabilities. (A) and (F) show contact matrices expected for random collisions; (B) and (G) show matrices predicted by the model; (C) and (H) show measured matrices [27]. (A)–(C) show contact probabilities integrated over chromosomes (corresponding to the probability that a contact occurs between any pair of chromosomes). (F–H) show averaged contact probabilities for each chromosome pair (probability per unit genomic length squared).

(D and I) Scatterplots of predicted versus measured contact frequencies. Each of the 136 dots corresponds to a distinct pair of chromosomes. Blue dots denote *trans* interactions, and red dots *cis* interactions. Pearson (*r*) and Spearman (*ρ*) correlation coefficients between predictions and measurements are indicated, for all contacts (black), *trans* contacts only (blue), or *cis* contacts only (red).

(E) Proportions of *cis* and *trans* contacts expected for random collisions, predicted by the model and measured. See Figure S3 for corresponding analyses of contacts between chromosome arms.

out-of-equilibrium fractal globule structure [9, 32]. The predicted $s^{-1.5}$ decay and the plateau above ~1,000 Kb agreed well with the measurements (Figure 4B).

The intrachromosomal contact frequency patterns predicted by the model were further characterized by a "negative cross" centered on the centromere, indicating a segregation of centromeric regions from the rest of the chromosome (Figure 4C; Figure S4A). This feature was also apparent in the experimental data (Figure 4D; Figure S4B). For chromosome 12, which carries the rDNA locus, the model predicted a striking dearth of contacts between the genomic regions on either side of the rDNA (Figure 4E). This was also observed in the Hi-C data [27] (Figure 4F).

Finally, we examined contacts between distinct chromosomes. The predicted contact patterns were mainly characterized by an enrichment between pericentromeric regions (Figure 4G; Figure S4A), in accordance with the Hi-C data

[27] (Figure 4H; Figure S4B). Our model also predicted a weaker negative cross pattern similar to that of intrachromosomal contacts, characterized by a depletion of contacts between centromeres and noncentromeric regions of other chromosomes (Figure 4G; Figure S4A). This feature was barely discernable in the much noisier experimental map (Figure 4H; Figure S4B), thus a confirmation of this prediction may require new Hi-C data.

Thus, our model is able to recapitulate the main observed patterns of contact frequencies at subchromosomal scales in both *cis* and *trans*.

Predicting Alterations of Nuclear Architecture
To test our model's predictive power, we sought to simulate an alteration of nuclear organization amenable to experimental verification. Given the prominence of the nucleolar compartment and its origin in the high transcription of rDNA, we
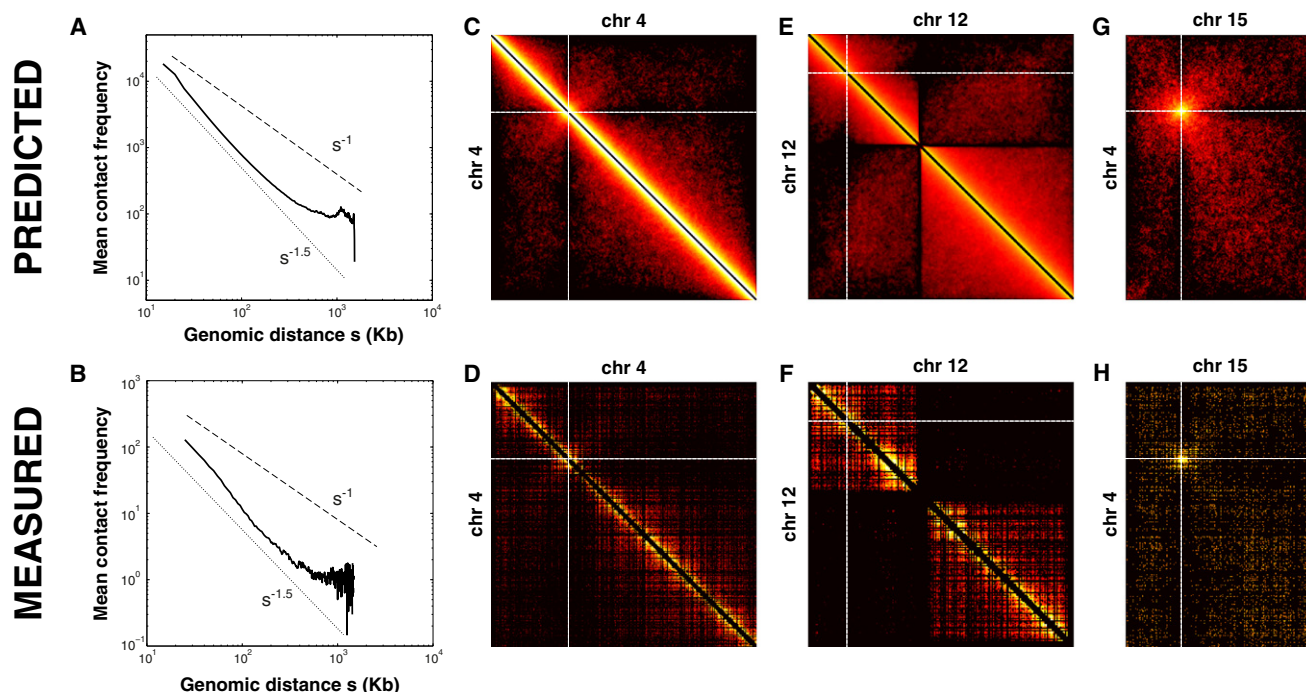
Figure 4. Model Recovers Subchromosomal Contact Patterns

(A, C, E, G) Model predictions. (B, D, F, H) Measurements. (A and B) The solid curve shows the average intrachromosomal contact frequency F as function of genomic separation s. The dotted and dashed lines indicate power laws s^{-1} and $s^{-1.5}$, respectively. Note the logarithmic scales. (C) and (D) show contact frequencies within chromosome 4; (E) and (F) show contacts within chromosome 12; (G) and (H) show contacts between chromosomes 4 and 15. All contact frequency matrices are shown using a logarithmic color scale. The dotted lines indicate the position of the centromeres. See Figure S4 for the entire genome-wide contact matrices.

analyzed how the model responded to a reduction in the transcriptional activity of this locus. This was previously achieved experimentally by treating cells with rapamycin, resulting in an approximate halving of the nucleolar volume [22]. To model this effect, we diminished the diameter of rDNA segments to D_{rDNA} = 140 nm. The predicted rDNA territory had a reduced volume but still resembled a crescent abutting the nuclear envelope opposite the SPB, in agreement with observations [22]. We analyzed the effect of the reduced nucleolus on the absolute and relative positions of telomeres (Figure 5). The model predicted that rapamycin treatment causes telomeres to extend to larger α than in absence of the drug and that the increase in α was larger for longer chromosome arms; this prediction was in good agreement with measurements for six telomeres whose arm lengths ranged from 85 Kb (Tel6R) to 1,050 Kb (Tel4R) [22] (Figures 5A–5M). The predicted and measured changes in α agreed well (r = 0.82, p = 0.0011) (Figure 5M). Similarly, the model predicted an increase in the distances of two telomere pairs (6R-3L and 6R-4R), in accordance with previous measurements [22] (Figure 5N). Thus, the model correctly predicted nuclear reorganization in response to a global change in rDNA transcription.

Discussion

We have presented a new computational model of global chromosome arrangements in the yeast nucleus. Unlike other recent models [27, 31, 34], ours did not rely on measured contact frequencies or light microscopy data, but instead used first principles and assumed few parameters all based on preexisting literature. The model represented chromosomes as confined (hetero)polymers undergoing passive Brownian dynamics, subject only to steric and topological constraints (Figure 1). We did not assume specific DNA binding factors, except implicitly through the assumption of modified chromatin properties at the rDNA locus and via the tethering of telomeres and centromeres. In contrast to other models designed for human cells [33, 35, 36], ours made no provisions for loops. We also did not assume any active motions. Despite this simplicity, the model accounts qualitatively and quantitatively for key aspects of yeast nuclear organization: the morphology and position of the nucleolus, its exclusion of all DNA except the rDNA, the nonrandom positions of genes and telomeres relative to nuclear landmarks and to each other (Figure 2), and patterns of contact frequencies across the genome, at the scale of chromosomes, chromosome arms, and at subchromosomal scales (Figures 3 and 4, Figures S3 and S4). Other models investigated here failed to explain all of these features simultaneously, although for some features the agreement was also good (Table 2; Figure S2). Our nominal model successfully predicted a change in nuclear organization in conditions of reduced rDNA gene expression (Figure 5). Nevertheless, it will be important to test its predictions in additional experiments that alter the mechanical constraints on chromosomes or chromosome structure or in other yeast species.

Our results have implications for the mechanisms governing nuclear organization in yeast. Although we cannot rule out specific interactions binding chromatin loci to each other or to nuclear landmarks besides centromeres and telomeres, our data suggest that such interactions are not required to explain global large-scale organization of the nucleus.
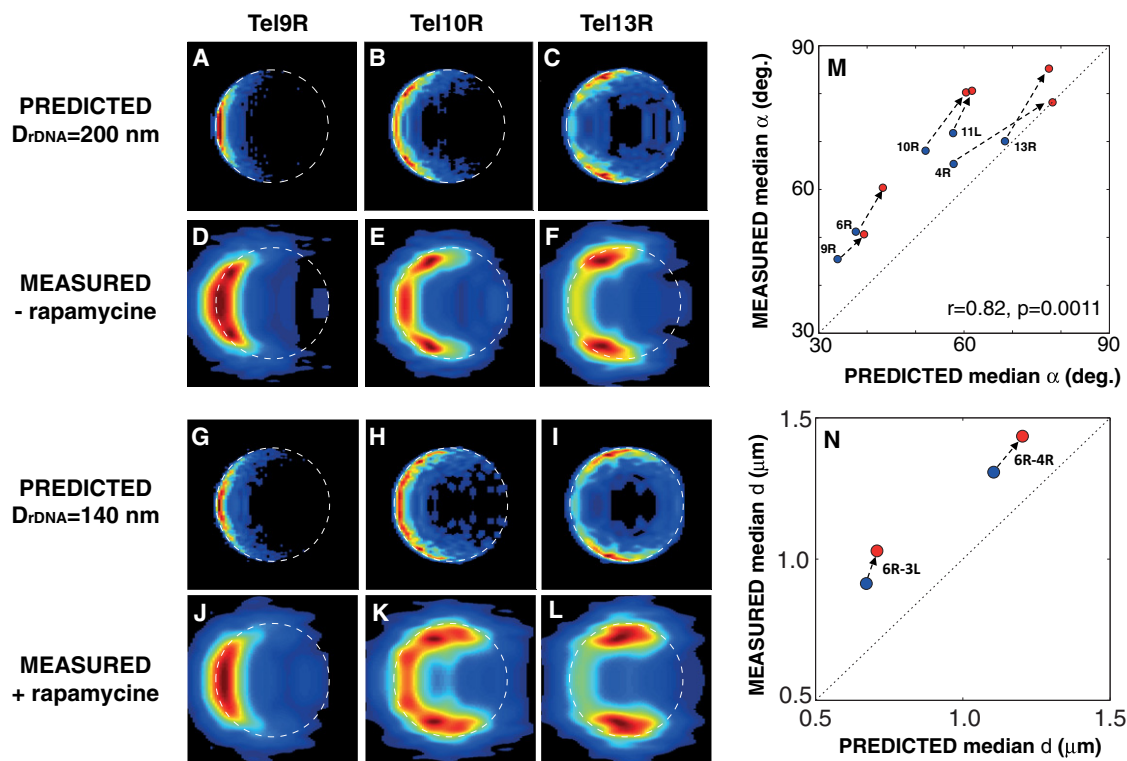
Figure 5. Model Predicts Alterations of Nuclear Organization under Reduced rDNA Transcription

(A–L) Intranuclear territories of three selected telomeres as predicted by the model (A–C and G–I) or measured [22] (D–F and J–L). (A)–(C) show predictions by the nominal model with D_{rDNA} = 200 nm. (D)–(F) show experimental measurements in absence of rapamycin [22]. (G)–(I) show predictions by the model with D_{rDNA} = 140 nm. (J)–(L) show experimental measurements in presence of rapamycin [22].

(M) Measured versus predicted median α of six telomeres in each condition.

(N) Predicted versus measured median distance between pairs of telomeres (6R, 3L) and (6R, 4R) in each condition. In (M) and (N), blue dots indicate absence of rapamycin or D_{rDNA} = 200, and red dots indicate presence of rapamycin or D_{rDNA} = 140 nm. Arrows indicate how values change upon treatment by rapamycin or reduction of D_{rDNA}. Note that the model correctly predicted an increase in α and in distances upon rapamycin treatment. See also Figure S5.

Similarly, our data suggest that no energy-dependent, e.g., molecular motor-driven, dynamics is required. Instead, our data support the notion that yeast nuclear organization can be understood by the sole properties of confined and topologically constrained polymers, combined with the tethering of centromeres and telomeres. More specifically, chromosome arrangements can be explained by entropic repulsion of topologically constrained chromosome arms [37], whereas the segregation of rDNA into a distinct nucleolar compartment is consistent with entropic phase separation of block heteropolymers [38] [39]. This agrees with the notion that nuclear bodies arise by self-organization rather than by assembling onto preexisting scaffolds [40]. Our results are also in agreement with the conclusions of a different computational study (published during revision of this manuscript), which, however, did not self-consistently model the nucleolar compartmentalization [41].

Despite our model's success in recapitulating global features of nuclear organization, we acknowledge several limitations. First, the agreement with measurements is statistical and imperfect. Thus, other combinations of poorly known parameters (such as *L*, *C*, and D_{rDNA} in Table 1) or other equally simple models may explain observations even better. Furthermore, the experimental data considered here have only moderate spatial and genomic resolutions, and are based on large cell populations. Accordingly, specific rather than generic factors may still govern chromatin folding at

smaller scales, or determine positions and dynamics of a subset of loci, or even exert global influence in a fraction of the cell population. Such specific factors may act during biological processes and underlie, e.g., the repositioning of inducible genes [3, 42] or the clustering of replication origins [43]. To address this, more systematic explorations of the simulation parameter space will likely help improve modeling, but new imaging or Hi-C data with better spatial and genomic resolution are essential. Notwithstanding, our model may already facilitate the identification of specific DNA interactions from experimental data by providing a means to predict the unspecific effects.

In higher eukaryotes, substantial evidence points to the role of DNA-specific factors in mediating interactions between distal loci and organizing chromosomes into distinct large-scale domains [16, 17, 44]. To account for such observations, computational models may need to include specific interactions, but it is likely that entropic effects and polymer properties also need to be considered to understand nuclear organization in these organisms [18, 33, 45].

At the functional level, our model is likely to have direct implications in understanding where chromosomal rearrangements (which require physical interactions between distal loci) are most likely to occur. In support of this, we analyzed 96 known chromosomal breakpoints and found that predicted contact frequencies at the observed breakpoints were significantly higher than expected if breakpoint loci were randomly located

in the genome (Table S2; Figure S5). More experimental data are needed to refine these results in various classes of events. Nevertheless, this first analysis suggests that the model might be used to identify chromosomal regions that may spontaneously interact to generate chromosomal rearrangements. In the future, the model may also be used to examine constraints on gene repositioning during gene expression, the interaction of mating type loci, the formation of replication foci, and other functionally important processes [42, 43, 46]. Overall, our model constitutes a framework to quantitatively understand and predict global features of nuclear organization and some of its functional consequences in this important model organism.

Experimental Procedures

Computational Model

The simulation used the open source physics engine (ODE), which allows one to model the dynamics of rigid bodies subject to external forces and constraints arising from collisions and joints between distinct bodies (www.ode.org). We represented each of the 16 haploid yeast chromosomes as freely jointed chains of cylinders (Figure 1A). The motion of each segment was governed by the discretized Langevin equation, which includes a randomly oriented force representing thermal agitation, and a viscous friction term, in addition to forces needed to respect the constraints arising from collisions and joints. The main parameters used in the model are listed in Table 1. In the homopolymer model, we assumed that the physical properties of chromatin are constant across the genome. Thus, the chains were uniquely characterized by only three parameters: cylinder length (Kuhn length L, in nm), which determines chain rigidity, cylinder diameter (D_0, in nm), and compaction, expressed as nucleotides per length (C, in bp/nm). The genomic length of each chromosome then uniquely determined the number of segments in each chain. Although the physical parameters (L, D_0, C) remain uncertain, we used values based on previous studies [47–49]. In the heteropolymer simulation, the N_{rDNA} segments corresponding to the rDNA locus were replaced by spheres of diameter D_{rDNA}. Except during the initial phase of the simulation (see below), we modeled the nuclear envelope as a sphere of radius $R_0 = 1$ μm, acting as an impenetrable boundary, and the SPB as a cylinder of diameter 120 nm embedded in the spherical shell (Figures 1C and 1D). We modeled each of the 16 microtubule + kinetochore complexes as a single cylinder of length $L_{MT} = 380$ nm and diameter 25 nm (Figure 1E) [50], of which one end remained in contact with the inner face of the SPB, whereas the other end was attached to the centromeric segment. To enforce telomere tethering to the nuclear envelope, we introduced a force that maintained the telomeric segments near the surface of the sphere without constraining their tangential motion. No other forces were introduced.

We initialized each simulation run with an artificial configuration in which chromosome chains were stretched out and parallel to each other, with their centromeres disposed at equal intervals along a circle of radius L_{MT} centered on the SPB, but in a random clockwise order (Figures S1A and S1B). To accommodate this initial configuration, we modeled the initial nuclear envelope as a long cylinder of radius R_0 capped by two half spheres (Figure S1A). During the initial phase of the simulation (3.5 10^5 time steps), which was not used to compute model predictions, the length of this cylinder was progressively reduced (Figure S1C), until the nuclear envelope was a sphere of radius R_0 embedding the SPB (Figure S1D). This initialization ensured that individual chains did not overlap and were not entangled with each other, as indeed the case for mitotic chromosomes. We plotted the time course of gyration radii and distances between chain extremities (telomeres) and verified that these quantities stabilized (i.e., fluctuated around a constant mean) before sampling the trajectories at large intervals (1 out of > 1,000 time steps taken after 10^6 time steps) (Figures S1E and S2G). We also checked that the autocorrelation of the sampled data was negligible for nonzero lags (Figures S1F and S1H). Finally, to increase the sample size without excessive simulation time, we aggregated predicted loci and contact data from ∼20 parallel simulation runs.

Strain Constructions and Microscopy

For fluorescent tagging of individual loci along chromosome 4 (Table S1), we constructed 16 new strains bearing Tet operator sequences near the locus of interest and expressing the repressor protein fused to GFP. Labeling of the nucleolus and nuclear pores and spinning disc fluorescence microscopy were performed as previously described [3, 22].

Breakpoint Analysis

We compiled a list of 96 breakpoints from the literature, which corresponded mainly to duplication and translocation events and included 38 homologous and 56 nonhomologous recombination events, 21 intrachromosomal and 75 interchromosomal events, and 49 events from haploid and 47 from diploid cells (Table S2). These data were selected from experiments imposing as little constraints as possible on the position of at least one of the two breakpoint loci.

Supplemental Information

Supplemental Information includes five figures, two tables, and one movie and can be found with this article online at http://dx.doi.org/10.1016/j.cub.2012.07.069.

References

1. Misteli, T. (2005). Concepts in nuclear architecture. Bioessays *27*, 477–487.
2. Cremer, T., and Cremer, M. (2010). Chromosome territories. Cold Spring Harb. Perspect. Biol. *2*, a003889.
3. Berger, A.B., Cabal, G.G., Fabre, E., Duong, T., Buc, H., Nehrbass, U., Olivo-Marin, J.C., Gadal, O., and Zimmer, C. (2008). High-resolution statistical mapping reveals gene territories in live yeast. Nat. Methods *5*, 1031–1037.
4. Heun, P., Laroche, T., Shimada, K., Furrer, P., and Gasser, S.M. (2001). Chromosome dynamics in the yeast interphase nucleus. Science *294*, 2181–2186.
5. Taddei, A., Schober, H., and Gasser, S.M. (2010). The budding yeast nucleus. Cold Spring Harb. Perspect. Biol. *2*, a000612.
6. Misteli, T. (2010). Higher-order genome organization in human disease. Cold Spring Harb. Perspect. Biol. *2*, a000794.
7. Wijchers, P.J., and de Laat, W. (2011). Genome organization influences partner selection for chromosomal rearrangements. Trends Genet. *27*, 63–71.
8. Hakim, O., Resch, W., Yamane, A., Klein, I., Kieffer-Kwon, K.R., Jankovic, M., Oliveira, T., Bothmer, A., Voss, T.C., Ansarah-Sobrinho, C., et al. (2012). DNA damage defines sites of recurrent chromosomal translocations in B lymphocytes. Nature *484*, 69–74.
9. Zhang, Y., McCord, R.P., Ho, Y.J., Lajoie, B.R., Hildebrand, D.G., Simon, A.C., Becker, M.S., Alt, F.W., and Dekker, J. (2012). Spatial organization of the mouse genome and its role in recurrent chromosomal translocations. Cell *148*, 908–921.
10. Chiarle, R., Zhang, Y., Frock, R.L., Lewis, S.M., Molinie, B., Ho, Y.J., Myers, D.R., Choi, V.W., Compagno, M., Malkin, D.J., et al. (2011). Genome-wide translocation sequencing reveals mechanisms of chromosome breaks and rearrangements in B cells. Cell *147*, 107–119.
11. Chambeyron, S., and Bickmore, W.A. (2004). Chromatin decondensation and nuclear reorganization of the HoxB locus upon induction of transcription. Genes Dev. *18*, 1119–1130.
12. Nagai, S., Dubrana, K., Tsai-Pflugfelder, M., Davidson, M.B., Roberts, T.M., Brown, G.W., Varela, E., Hediger, F., Gasser, S.M., and Krogan, N.J. (2008). Functional targeting of DNA damage to a nuclear pore-associated SUMO-dependent ubiquitin ligase. Science *322*, 597–602.

13. Miné-Hattab, J., and Rothstein, R. (2012). Increased chromosome mobility facilitates homology search during recombination. Nat. Cell Biol. *14*, 510–517.

14. Dion, V., Kalck, V., Horigome, C., Towbin, B.D., and Gasser, S.M. (2012). Increased mobility of double-strand breaks requires Mec1, Rad9 and the homologous recombination machinery. Nat. Cell Biol. *14*, 502–509.

15. Zimmer, C., and Fabre, E. (2011). Principles of chromosomal organization: lessons from yeast. J. Cell Biol. *192*, 723–733.

16. Phillips, J.E., and Corces, V.G. (2009). CTCF: master weaver of the genome. Cell *137*, 1194–1211.

17. Sexton, T., Yaffe, E., Kenigsberg, E., Bantignies, F., Leblanc, B., Hoichman, M., Parrinello, H., Tanay, A., and Cavalli, G. (2012). Three-dimensional folding and functional organization principles of the Drosophila genome. Cell *148*, 458–472.

18. Rosa, A., and Everaers, R. (2008). Structure and dynamics of interphase chromosomes. PLoS Comput. Biol. *4*, e1000153.

19. Marenduzzo, D., Micheletti, C., and Cook, P.R. (2006). Entropy-driven genome organization. Biophys. J. *90*, 3712–3721.

20. Léger-Silvestre, I., Trumtel, S., Noaillac-Depeyre, J., and Gas, N. (1999). Functional compartmentalization of the nucleus in the budding yeast Saccharomyces cerevisiae. Chromosoma *108*, 103–113.

21. Bystricky, K., Laroche, T., van Houwe, G., Blaszczyk, M., and Gasser, S.M. (2005). Chromosome looping in yeast: telomere pairing and coordinated movement reflect anchoring efficiency and territorial organization. J. Cell Biol. *168*, 375–387.

22. Thérizols, P., Duong, T., Dujon, B., Zimmer, C., and Fabre, E. (2010). Chromosome arm length and nuclear constraints determine the dynamic relationship of yeast subtelomeres. Proc. Natl. Acad. Sci. USA *107*, 2025–2030.

23. Marshall, W.F., Straight, A., Marko, J.F., Swedlow, J., Dernburg, A., Belmont, A., Murray, A.W., Agard, D.A., and Sedat, J.W. (1997). Interphase chromosomes undergo constrained diffusional motion in living cells. Curr. Biol. *7*, 930–939.

24. Heun, P., Laroche, T., Raghuraman, M.K., and Gasser, S.M. (2001). The positioning and dynamics of origins of replication in the budding yeast nucleus. J. Cell Biol. *152*, 385–400.

25. Schober, H., Kalck, V., Vega-Palas, M.A., Van Houwe, G., Sage, D., Unser, M., Gartenberg, M.R., and Gasser, S.M. (2008). Controlled exchange of chromosomal arms reveals principles driving telomere interactions in yeast. Genome Res. *18*, 261–271.

26. Dekker, J., Rippe, K., Dekker, M., and Kleckner, N. (2002). Capturing chromosome conformation. Science *295*, 1306–1311.

27. Duan, Z., Andronescu, M., Schutz, K., McIlwain, S., Kim, Y.J., Lee, C., Shendure, J., Fields, S., Blau, C.A., and Noble, W.S. (2010). A three-dimensional model of the yeast genome. Nature *465*, 363–367.

28. Rabl, C. (1885). über Zellteilung. Morphologisches Jahrbuch *10*, 214–330.

29. Hediger, F., Neumann, F.R., Van Houwe, G., Dubrana, K., and Gasser, S.M. (2002). Live imaging of telomeres: yKu and Sir proteins define redundant telomere-anchoring pathways in yeast. Curr. Biol. *12*, 2076–2089.

30. Haeusler, R.A., and Engelke, D.R. (2004). Genome organization in three dimensions: thinking outside the line. Cell Cycle *3*, 273–275.

31. Tokuda, N., Terada, T.P., and Sasai, M. (2012). Dynamical modeling of three-dimensional genome organization in interphase budding yeast. Biophys. J. *102*, 296–304.

32. Lieberman-Aiden, E., van Berkum, N.L., Williams, L., Imakaev, M., Ragoczy, T., Telling, A., Amit, I., Lajoie, B.R., Sabo, P.J., Dorschner, M.O., et al. (2009). Comprehensive mapping of long-range interactions reveals folding principles of the human genome. Science *326*, 289–293.

33. Rosa, A., Becker, N.B., and Everaers, R. (2010). Looping probabilities in model interphase chromosomes. Biophys. J. *98*, 2410–2419.

34. Kalhor, R., Tjong, H., Jayathilaka, N., Alber, F., and Chen, L. (2012). Genome architectures revealed by tethered chromosome conformation capture and population-based modeling. Nat. Biotechnol. *30*, 90–98.

35. Münkel, C., Eils, R., Dietzel, S., Zink, D., Mehring, C., Wedemann, G., Cremer, T., and Langowski, J. (1999). Compartmentalization of interphase chromosomes observed in simulation and experiment. J. Mol. Biol. *285*, 1053–1065.

36. Mateos-Langerak, J., Bohn, M., de Leeuw, W., Giromus, O., Manders, E.M.M., Verschure, P.J., Indemans, M.H.G., Gierman, H.J., Heermann, D.W., van Driel, R., and Goetze, S. (2009). Spatially confined folding of chromatin in the interphase nucleus. Proc. Natl. Acad. Sci. USA *106*, 3812–3817.

37. De Gennes, P.G. (1980). Conformations of polymers attached to an interface. Macromolecules *13*, 1069–1075.

38. Leibler, L. (1980). Theory of microphase separation in block copolymers. Macromolecules *13*, 1602–1617.

39. Cook, P.R., and Marenduzzo, D. (2009). Entropic organization of interphase chromosomes. J. Cell Biol. *186*, 825–834.

40. Misteli, T. (2001). The concept of self-organization in cellular architecture. J. Cell Biol. *155*, 181–185.

41. Tjong, H., Gong, K., Chen, L., and Alber, F. (2012). Physical tethering and volume exclusion determine higher-order genome organization in budding yeast. Genome Res. *22*, 1295–1305.

42. Cabal, G.G., Genovesio, A., Rodriguez-Navarro, S., Zimmer, C., Gadal, O., Lesne, A., Buc, H., Feuerbach-Fournier, F., Olivo-Marin, J.C., Hurt, E.C., and Nehrbass, U. (2006). SAGA interacting factors confine sub-diffusion of transcribed genes to the nuclear envelope. Nature *441*, 770–773.

43. Knott, S.R., Peace, J.M., Ostrow, A.Z., Gan, Y., Rex, A.E., Viggiani, C.J., Tavaré, S., and Aparicio, O.M. (2012). Forkhead transcription factors establish origin timing and long-range clustering in S. cerevisiae. Cell *148*, 99–111.

44. Dixon, J.R., Selvaraj, S., Yue, F., Kim, A., Li, Y., Shen, Y., Hu, M., Liu, J.S., and Ren, B. (2012). Topological domains in mammalian genomes identified by analysis of chromatin interactions. Nature *485*, 376–380.

45. Finan, K., Cook, P.R., and Marenduzzo, D. (2011). Non-specific (entropic) forces as major determinants of the structure of mammalian chromosomes. Chromosome research: an international journal on the molecular, supramolecular and evolutionary aspects of chromosome biology *19*, 53–61.

46. Bressan, D.A., Vazquez, J., and Haber, J.E. (2004). Mating type-dependent constraints on the mobility of the left arm of yeast chromosome III. J. Cell Biol. *164*, 361–371.

47. Dekker, J. (2008). Mapping in vivo chromatin interactions in yeast suggests an extended chromatin fiber with regional variation in compaction. J. Biol. Chem. *283*, 34532–34540.

48. Schalch, T., Duda, S., Sargent, D.F., and Richmond, T.J. (2005). X-ray structure of a tetranucleosome and its implications for the chromatin fibre. Nature *436*, 138–141.

49. Cui, Y., and Denis, C.L. (2003). In vivo evidence that defects in the transcriptional elongation factors RPB2, TFIIS, and SPT5 enhance upstream poly(A) site utilization. Mol. Cell. Biol. *23*, 7887–7901.

50. O'Toole, E.T., Winey, M., and McIntosh, J.R. (1999). High-voltage electron tomography of spindle pole bodies and early mitotic spindles in the yeast Saccharomyces cerevisiae. Mol. Biol. Cell *10*, 2017–2031.